PAPER

Check for updates

A vapor-phase-assisted growth route for large-scale uniform deposition of MoS₂ monolayer films†

Devendra Pareek, [ID] ‡*[a] Marco A. Gonzalez,‡[a] Jannik Zohrabian,[a]
Mohamed H. Sayed, [ID] §[a] Volker Steenhoff,[b] Colleen Lattyak, [ID] [b] Martin Vehse,[b]
Carsten Agert,[b] Jürgen Parisi,[a] Sascha Schäfer[a] and Levent Gütay [ID] [a]

In this work a vapor-phase-assisted approach for the synthesis of monolayer MoS₂ is demonstrated, based on the sulfurization of thin MoO₃₋ₓ precursor films in an H₂S atmosphere. We discuss the co-existence of various possible growth mechanisms, involving solid–gas and vapor–gas reactions. Different sequences were applied in order to control the growth mechanism and to obtain monolayer films. These variations include the sample temperature and a time delay for the injection of H₂S into the reaction chamber. The optimized combination allows for tuning the process route towards the potentially more favorable vapor–gas reactions, leading to an improved material distribution on the substrate surface. Raman and photoluminescence (PL) spectroscopy confirm the formation of ultrathin MoS₂ films on SiO₂/Si substrates with a narrow thickness distribution in the monolayer range on length scales of a few millimeters. Best results are achieved in a temperature range of 950–1000 °C showing improved uniformity in terms of Raman and PL line shapes. The obtained films exhibit a PL yield similar to mechanically exfoliated monolayer flakes, demonstrating the high optical quality of the prepared layers.

Introduction

Recently there has been considerable interest in the synthesis and investigation of novel two-dimensional semiconducting materials, such as transition metal dichalcogenides (TMDC), for application in next-generation ultrathin and flexible electronics.[1–5] As one of the most widely studied TMDC materials, MoS₂ shows unique optical and electronic properties, occurring as a result of quantum confinement and decreased screening when the films are reduced to a quasi-two-dimensional monolayer structure. Considerable efforts have been made to achieve monolayer films, particularly using processes that are compatible with state-of-the-art industrial fabrication technologies. Chemical Vapor Deposition (CVD), for example, is an established fabrication process and a promising approach for large area deposition of ultrathin TMDC films.[6] However, 2D MoS₂ layers from mechanical exfoliation show better mobility and electronic characteristics when compared to CVD-processed layers.[7–10] High mobilities up to 30 cm² V⁻¹ s⁻¹ were achieved

by MO-CVD processes, which are also promising for large area deposition approaches.[11,12]

Although remarkable efforts have been made for developing bottom-up deposition approaches,[13–15] the understanding of the reaction and growth mechanisms are still at an early stage. Thus, growing closed layers on areas above the hundred μm range with opto-electronic quality comparable to that of exfoliated flakes remains a challenge.[10,16–18] This strongly requires strategies apart from the conventional CVD approaches, which rely on the sulfurization of various Mo-precursors at a thermodynamically suitable temperature and pressure combination[7,8,16–18] and allow for only a moderate control on the spontaneous growth of layers or islands.

The formation of high-quality monolayers can be considered to include two key aspects, namely the synthesis reaction of MoS₂, and its homogenous distribution on the substrate surface. These two steps may happen simultaneously but should be addressed separately by means of an additional process parameter, so that an improved control on the layer thickness is achieved.

In this work, we present a vapor-phase-assisted growth approach for the synthesis of MoS₂ films in the monolayer regime, which includes the rapid heating of pre-deposited MoO₃₋ₓ precursor films and the subsequent sulfurization using H₂S gas. We show the control on layer thickness by introduction of an additional process parameter, which is the timing of H₂S exposure of the MoO₃₋ₓ precursor film, resulting in a quasi-kinetic process control regime. The optimization of

[a]*Institute of Physics, Carl von Ossietzky University of Oldenburg, Oldenburg, Germany. E-mail: devendra.pareek@uni-oldenburg.de*

[b]*DLR Institute of Networked Energy Systems, Oldenburg, Germany*

† Electronic supplementary information (ESI) available. See DOI: 10.1039/c8ra08626e

‡ Authors contributed equally to this work.

§ Current Address: Solid State Physics Department, National Research Centre, 12311 Dokki, Giza, Egypt

this parameter along with the appropriate temperature and pressure combination allows for reproducible growth of MoS_2 monolayers. Our optical and structural investigations demonstrate the coverage of the substrate surface over sample areas up to the mm scales.

Experimental section

MoO_{3-x} precursor films of various thicknesses were grown by electron-beam evaporation on: (i) native oxide covered bare Si substrates and (ii) 100 nm SiO_2 coated Si substrates. The substrates were placed face down above the MoO_3 source in a rotating substrate holder to improve deposition homogeneity. Evaporation was performed in an argon atmosphere at a pressure of 5×10^{-4} mbar (background pressure smaller than 10^{-5} mbar). The power of the electron-beam was controlled by a PID loop to maintain a deposition rate of ~ 0.3 Å s^{-1}, measured by a quartz crystal microbalance. A mechanical shutter was used to limit the deposition duration and obtain the desired nominal thickness. Sulfurization of the MoO_{3-x} layer was performed in a rapid thermal processing system (RTP, Annealsys AS-one 150) with the substrate placed face-up on a graphite susceptor, while heated from the top. After five pump/purge cycles with N_2 to remove air and moisture, the RTP chamber was pumped down to about 0.01 mbar, which is the common starting point for the entire set of experiments described in the following. The further process consists of two main parts, which are (i) injection of a H_2S/N_2 gas mixture (5%/95%) and (ii) a reactive annealing step. Process parameters, such as the relative timing of both parts and the annealing temperature, determine the type of the reaction mechanism and resulting material characteristics, as detailed later.

The H_2S/N_2 gas injection was performed until a reactor pressure of 60 mbar was reached (duration about 2 min at a flow rate of 117 sccm). After reaching a pressure of 60 mbar, a constant H_2S/N_2 flow of 20 sccm was kept until the end of the reaction process, during which the pressure was maintained constant using a closed-loop-controlled throttle valve.

During the annealing step the chamber was heated to a preset target temperature (650–1000 °C) at a ramp rate of 3 °C s^{-1}. The temperature was measured at the graphite susceptor by a thermocouple. The holding time for the main reaction process after reaching the desired pressure and temperature was set to 10 minutes. At the end of the process, the heating and the gas flow were switched off and the sample was left to cool down to ~ 150 °C inside the chamber. Finally, a N_2 purge/pump cycle was realized to decontaminate the chamber and to bring it to atmospheric pressure.

Raman and photoluminescence (PL) spectroscopy of the samples were performed in a Horiba LabRAM Aramis confocal microscopy setup with an excitation wavelength of 457.9 nm and a spot size of approximately 1 μm. For a quantitative evaluation of the optical properties of the prepared layers, additional reference samples were prepared by mechanical exfoliation of natural MoS_2 crystals, using a deterministic all-dry stamping method.[19]

Results and discussion

For understanding the MoS_2 formation and achieving the growth of ultrathin films, we synthesized MoS_2 films on bare silicon substrates, starting from MoO_{3-x} precursor layers of various thickness (0.6, 1.5 and 2.0 nm) at an annealing temperature of 700 °C.

Different process sequences were chosen, varying the timing of the H_2S gas injection and the temperature of reactive annealing. In terms of H_2S injection times, these sequences are defined as follows:

(a) At the start of the process at room temperature (process-a).

(b) At a target temperature of 700 °C (process-b).

(c) After a delay of 10 s when the target temperature of 700 °C was reached (process-c).

These process sequences can be considered to result in three different classes for the reaction process, moving from a conventional solid-state annealing process towards a vapor-phase-assisted process, which will be explained in detail further below.

Raman spectra were recorded on all synthesized samples which exhibit ubiquitously two characteristic peaks corresponding to two different phonon modes,[20–22] involving the out-of-plane vibration of S atoms (A_{1g}) at about 407–408 cm^{-1} and the in-plane vibration of Mo and S atoms (E^1_{2g}) at 385–387 cm^{-1}, with a peak distance δ in the range of 20–25 cm^{-1}. Raman labels are used according to the space-group of the bulk material.[23] As described in the literature,[20–22] the Raman peak distance can be used to determine the number of layers in MoS_2 films. In particular, for silicon oxide substrates, δ-values below 20.7 cm^{-1} indicate a monolayer, and values up to 22.2 cm^{-1} and 23.8 cm^{-1} correspond to two- and three-layer films, respectively.

Fig. 1(a) shows the Raman peak distances for all samples produced in the series mentioned above. Here, in the following, δ-values are given as the average over at least 5 measurement positions on each sample, the corresponding error bar indicates the spread of δ-values, as a measure for the homogeneity of the samples. The results confirm that thinner precursors result in MoS_2 films with fewer layers. Furthermore, a general trend towards lower values can be observed moving from process-a towards process-c. In particular, all the samples prepared via process-a show δ-values corresponding to two or more layers. In case of process-b and process-c, the samples prepared using thicker MoO_{3-x} layers, contain two or three MoS_2 layers. In contrast, when using a nominal precursor thickness of 0.6 nm, the obtained Raman peak separation matches the values reported for MoS_2 monolayers.[24]

To further confirm that films with a monolayer thickness were synthesized, PL measurements were performed. The expected main PL peak position for monolayer MoS_2 at room temperature is reported to be between 1.82–1.89 eV,[24] depending on the environment, substrate and synthesis technique.[25] In addition to the peak position, PL intensity of MoS_2 films increases drastically as the number of layers decreases to a monolayer due to the evolution of the band gap from an indirect to a direct transition.[26]
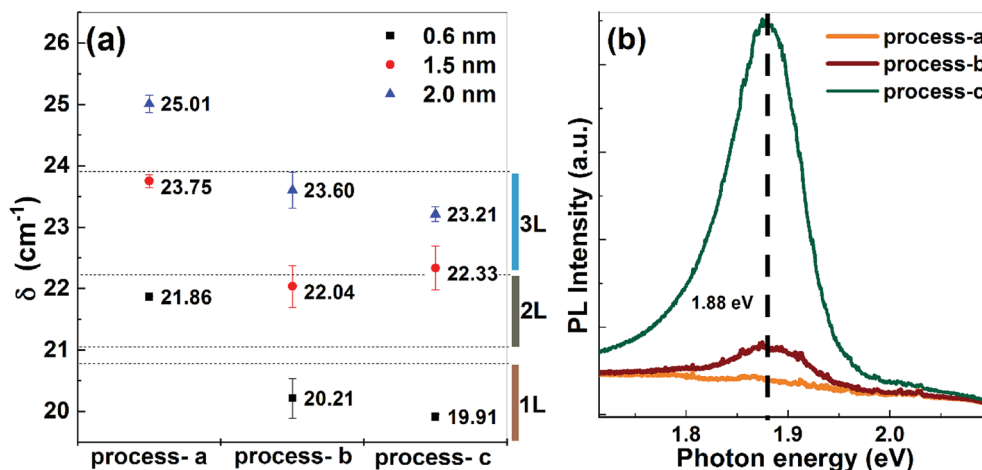
Fig. 1 (a) Peak separation (δ) between Raman modes A_{1g} and E_{2g}^1 for the samples prepared at 700 °C with different process sequences (process–a/b/c); (b) PL spectra of MoS_2 films produced *via* different process sequences using 0.6 nm thick MoO_{3-x} on Si substrate.

In Fig. 1(b) the PL spectra for MoS_2 samples processed from the 0.6 nm thick MoO_{3-x} precursors are depicted. The spectra show a strong increase of the PL intensity at a peak position of ~1.88 eV comparing samples prepared by process-a, -b and -c. These results clearly corroborate the existence of MoS_2 monolayers obtained from the 0.6 nm MoO_{3-x} precursor films using process-c. For the samples prepared by process-a and -b, low PL yields are obtained, which, in the case of process-a, further supports the formation of multiple MoS_2 layers. In the case of process-b, the PL intensity is unexpectedly low, although Raman results indicate monolayer films. Reduced PL yield might be connected to the co-existence of mono- and bilayer films or could be result of a high defect density, leading to efficient non-radiative recombination channels.

To further investigate the effect of the H_2S injection delay as well as the effect of process temperature on the MoS_2 formation and layer growth, we performed a detailed experimentation on 0.6 nm MoO_{3-x} precursor films at different target temperatures and with different H_2S injection times. All experiments were carried out with the same heating rate of 3 °C s^{-1}. The H_2S injection started with a delay of 0 s and 10 s after reaching the desired temperature, corresponding to process-b and process-c, respectively.

In Fig. 2(a), the resulting δ values are shown for various temperatures and injection delays. For the samples processed at 650 °C, the Raman peak separation indicates the formation of 2 to 3 layers of MoS_2. The corresponding PL (Fig. 2(b)) supports these findings. Samples prepared at 700 °C, were discussed in the previous section. At 750 °C, both samples show clear indication of monolayer formation both from Raman and PL, indicating a stable processing region.

At higher temperature ($T = 800$ °C), the sample shows Raman and PL spectra corresponding to monolayer MoS_2, but with a slight increase in Raman peak distance and decreased PL yield for delayed H_2S injection times. We note that the Si substrate with native oxide becomes unstable under H_2S atmosphere at temperatures exceeding 800 °C, and reaction products (potentially SiS_x[27]) are formed at the substrate edges.

In addition, cracks and imperfections are visible on the substrate. This surface deterioration at higher temperatures can be expected to affect the characteristics of the resulting MoS_2 films, which may lead to a higher δ-value and reduced PL intensity.

Since in the literature[28] best MoS_2 layer qualities are commonly achieved at process temperatures higher than 800 °C, we performed additional experiments on Si substrates with a defined SiO_2 layer (100 nm layer thickness). These substrates show a better thermal stability than the surface of bare Si wafers and can be processed at up to 950 °C without surface deterioration. The samples prepared (using process-b) in the temperature range of 750–900 °C exhibit Raman and PL spectra mainly in the monolayer regime, but with slight variations within each sample, which can be explained by inhomogeneous growth of MoS_2 on the substrate. The samples processed at 950 and 1000 °C (using process-b) appear to be homogeneous within the detection limits of the used confocal microscopy setup. This is illustrated in Fig. 3, which shows Raman and PL spectra taken at the corners and at the center of
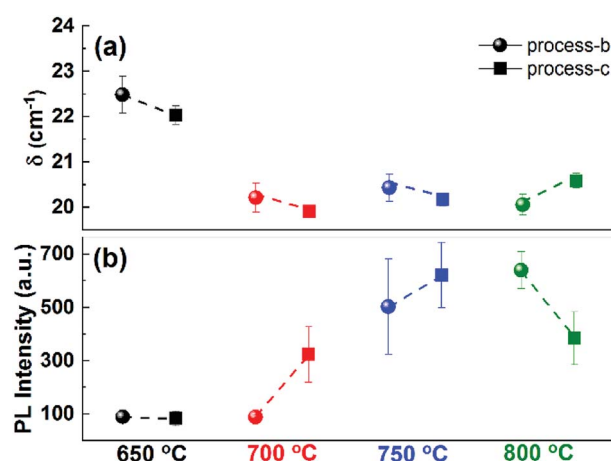

Fig. 2 (a) Raman peak spacing δ, and (b) PL intensity for the samples prepared at different processing temperatures, with (process–c), and without (process–b) H_2S injection delay.

each of these samples, which are 5 mm × 5 mm in size. As shown in Fig. 3(a) and (c), the Raman peak spacing for both samples is in good agreement with that of monolayer MoS_2. In Fig. 3(b) and (d) the PL spectra for both samples are plotted together with a spectrum from an exfoliated MoS_2 monolayer flake. We note that PL intensities of MoS_2 monolayers on SiO_2/Si substrates are about one order of magnitude higher compared to samples on bare silicon substrates. In fact, the MoS_2 films prepared on SiO_2/Si show a comparable PL intensity to exfoliated monolayers. In the inset of Fig. 3(b) and (d), the shape of the PL peaks is clearly visible and the location of the peaks are 1.86–1.89 eV and a shoulder around 2.05 eV, which is consistent with the reported PL peak position for monolayer MoS_2 synthesized by CVD techniques.[29–32] The graphs show a very similar peak shape for exfoliated and as-grown monolayers, and the peak position for the 1000 °C samples matches nicely with the PL from the exfoliated sample.

For exfoliated flakes, the intensity ratio $r = I(A_{1g})/I(E_{2g})$ of the two Raman peaks is in the range of one, and flakes exhibiting $r > 1$ were shown to contain sulfur vacancies.[33,34] MoS_2 monolayers grown by bottom-up approaches typically show r-values significantly higher than one.[11,13] In our samples, we find $r \approx 1.7$ at the highest process temperature of 1000 °C. Notably, we observe the highest PL intensity for the sample with the lowest r-value, supporting the notion that the Raman intensity ratio is a valuable measure for crystal quality. However, it is not immediately obvious up to what extent; spectroscopic correlations developed for exfoliated flakes can be quantitatively applied to grown nanocrystalline films.

To investigate the homogeneity of the MoS_2 layers not only on the mm scales but also on the micrometer scale, a Raman mapping was performed on the sample processed at 950 °C. Fig. 4(a) shows the variation in the δ value on an area of 40 × 40 μm. An area with a surface artifact was intentionally chosen to facilitate a reproducible selection of the investigated region on the sample. A PL mapping (Fig. 4(b)) performed in the same region confirms the homogeneity and high PL yield for the entire area. In the ESI,† scanning electron micrographs as well as an optical overview image are provided.

In the following, we will discuss our findings on the basis of different reaction and growth mechanisms. MoS_2 synthesis from MoO_3 is usually considered as a two-step process comprising partial reduction of MoO_3 into MoO_{3-x} under a reducing atmosphere, e.g. using H_2, at $T \sim 500$–600 °C followed by sulfurization, e.g. using S, at $T \sim 850$–1000 °C.[18,28,35] Studies also suggest that the MoS_2 films produced by a direct one-step sulfurization (i.e. without the intermediate step of partial reduction of MoO_3 under H_2 gas) were of inferior quality in terms of electrical properties.[18] In the present work, the H_2S gas, used as a sulfur source, has the beneficial side effect to further reduce the oxidation state of the evaporated MoO_{3-x} films. The processing was performed in the range of the
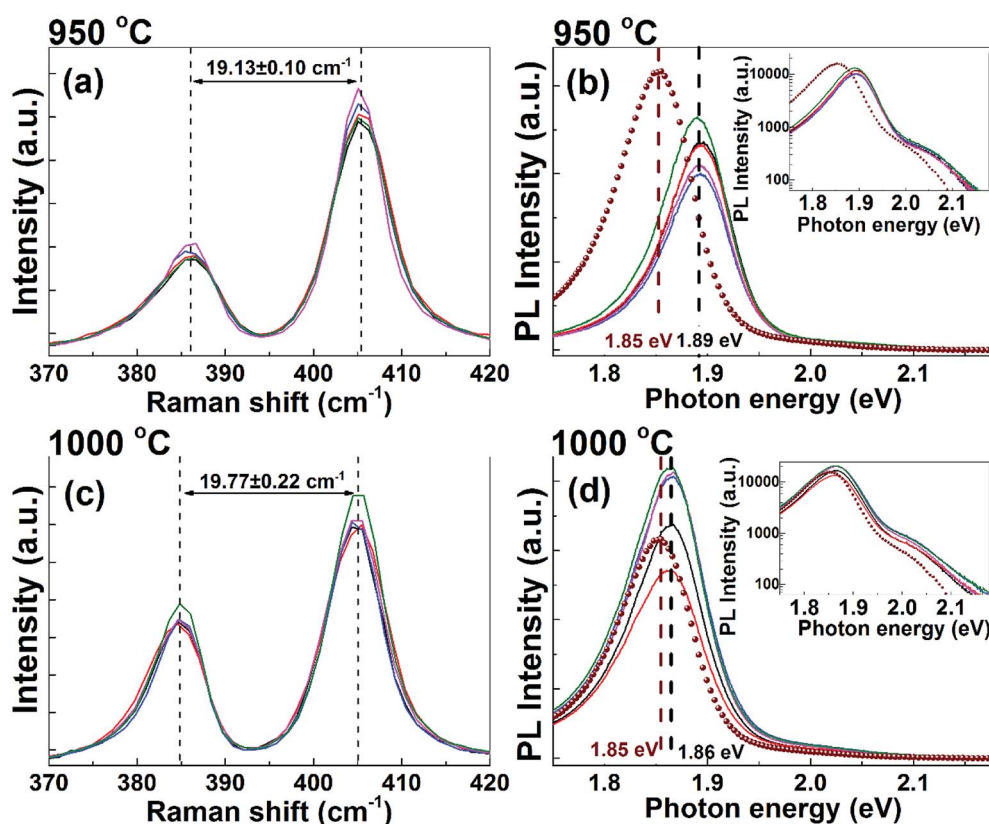

Fig. 3 Raman (a and c) and PL (b and d) spectra of MoS_2 samples prepared at 950 °C (a and b) and 1000 °C (c and d) on SiO_2/Si. Each graph shows measurements taken at 5 different positions on a 5 mm × 5 mm sample. Results obtained for an exfoliated MoS_2 monolayer flake are shown as dotted lines. Insets in (b and d): PL spectra on a logarithmic scale.
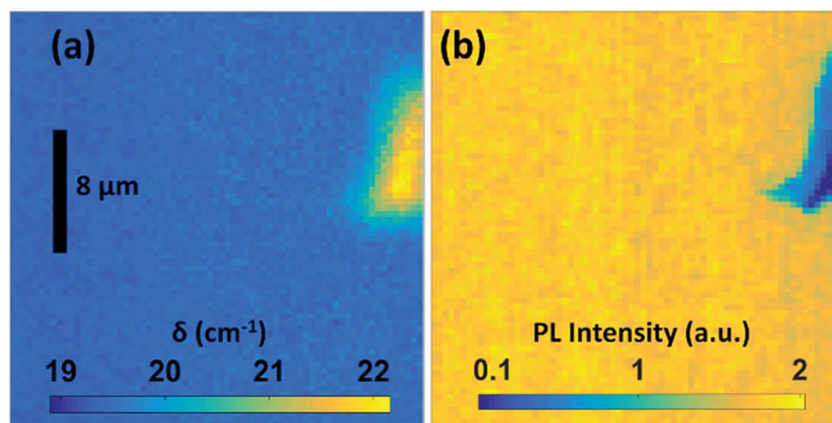
Fig. 4 Spatial map of Raman peak distance (a) and PL (b) recorded on a MoS_2 sample prepared at 950 °C.

decomposition temperature of H_2S, so that a mixture of H_2, S and H_2S (abbreviated as H_2S/S) is expected to be present in the chamber (at $T = 650$ °C the total conversion of H_2S to H_2 and S is about 10% [36,37]).

Furthermore, at the employed process temperatures ($T \geq 650$ °C), MoO_3 is considered to evaporate.[38,39] In agreement with this physical picture, longer waiting times before H_2S injection, *i.e.* going from process-a to -b and -c, and temperatures above 650 °C (*cf.* Fig. 1 and 2) result in thinner MoS_2 layers due to intermediate evaporation. We note that for the chosen temperature ramp and a process at 750 °C (Fig. 2, blue data), the sample already was at a temperature above 650 °C for 33–43 s at the time of H_2S injection, so that significant MoO_{3-x} evaporation is expected before the reaction initiates. MoO_{3-x} atomic layers directly bonded to the substrate may show a higher evaporation temperature as compared with MoO_{3-x} bulk material, resulting in a self-limiting evaporation similar as in atomic layer deposition approaches.

This statement indeed raises a further question: does the evaporated MoO_{3-x} get lost from the process environment or does it play a role in the further film formation by acting as a vapor phase precursor for the synthesis of MoS_2? To address this crucial question, we placed a small piece of substrate, which was coated with the MoO_{3-x} precursor in face-up orientation on a blank substrate. We conducted the experiment as process-b sequence at various temperatures and found a clear MoS_2 Raman signal on the previously blank substrate in the region adjacent to the precursor covered substrate. This outcome clearly confirms the presence of a CVD like vapor phase transport or reaction mechanism involving MoO_{3-x} vapor and H_2S/S. This experiment was repeated on a silicon substrate (at a susceptor temperature of 850 °C) with a 280 nm SiO_2 coating, which is known to have better optical contrast for visualization of MoS_2.[40] Fig. 5(a) and (b) show the optical image of the previously blank substrate after the process and the placement of the precursor containing substrate on top of the larger blank substrate, respectively. Blue regions visible in Fig. 5(a) correspond to areas in which a clear MoS_2 Raman signal is observed.

Summarizing the discussion above, including the reaction sequence yielding MoS_2, the evaporation of MoO_{3-x}, the observed vapor phase reaction for MoS_2 deposition, and the possible reaction pathways reported in literature,[35,38] we can state that the presented process involve the following reaction mechanisms:

(a) Reaction of solid MoO_{3-x} layers with H_2S/S to form MoS_2 layer (reaction pathway-1).

(b) Reaction of vapor phase MoO_{3-x} with H_2S/S to form MoS_2, which adsorbs and grows on the substrate (reaction pathway-2).

(c) Re-adsorption and diffusion of vapor phase MoO_{3-x} on the substrate and reaction in the solid phase with H_2S/S to form the MoS_2 on the substrate (reaction pathway-3).

Despite the general possibility of all these reaction pathways taking place at the same time, we can discern different probabilities for these routes for different process parameters. In case of process-a (see Fig. 1), when H_2S is available from the beginning of the process, the reaction of MoO_{3-x} with H_2S can start already even at $T < 400$ °C,[41] which is significantly below the evaporation temperature of MoO_{3-x}. Therefore, all samples prepared up to 650 °C can be considered to follow mainly reaction pathway-1. Even at 700 °C, for which the evaporation
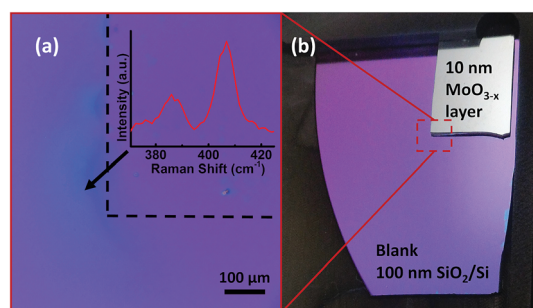

Fig. 5 (a) Contrast-enhanced optical image of the MoS_2 film coated on the SiO_2/Si substrate, indicating significant contributions from a vapor-phase assisted reaction pathway; arrow indicates the measurement region of the Raman spectrum shown in inset; (b) arrangement of the MoO_{3-x}-coated substrate on the blank substrate. The red box represents the region shown in (a).

temperature of MoO_{3-x} is just crossed, the sample would also predominantly react through reaction pathway-1, *i.e.* with sulfurization occurring before significant evaporation.

This is drastically changed in case of process-b and process-c, since the H_2S gas was not injected before reaching the desired process temperature, so that a noticeable amount of MoO_{3-x} would be already evaporated. This drives the reaction type from pathway-1 towards pathway-2 and -3, especially for higher temperatures and/or later injection times. In accordance to this description we do not see a noticeable difference between process-b and -c for the 0.6 nm sample for the process temperature of 650 °C, which both give a δ value of about 22 cm^{-1}. Here the main reaction takes place most likely *via* pathway-1.

In case of 700 °C susceptor temperature and process-b or process-c the reaction was accordingly pushed further towards pathway-2 and pathway-3, assumingly still keeping a fraction of pathway-1 in the process. Already at 0 s injection delay (process-b) a significant amount of MoO_{3-x} is evaporated to result in a δ value in the range of monolayer (even if PL did not confirm this clearly, see above). An injection delay of 10 s (process-c) resulted in a clear monolayer signal both from Raman and PL, as the process was pushed further towards pathway-2 and -3 and away from pathway-1. For the discussed results at 750 °C and above the same arguments are valid, leading to a stronger fraction of pathways-2 and 3 compared to pathway-1. It is important to note that higher temperatures, longer H_2S injection delays, and different pressure conditions can lead to an escape of the precursor vapour from the vicinity of the substrate surface, preventing the formation of MoS_2 layers.

It is expected that pathway-2 and -3 result in a more homogeneous distribution of MoS_2 on the substrate, compared to pathway-1. In case of pathway-1, the homogeneity and thickness of MoS_2 is directly influenced by the corresponding properties of the MoO_{3-x} precursor layer. For pathways-2 and -3, a rather homogeneous distribution of the reactants occurs through the vapor phase, leading to MoS_2 film quality largely independent from the initial MoO_{3-x} film morphology.

An interesting aspect for future works concerns the nanoscale morphology of the prepared monolayers. Although we could demonstrate homogeneous optical properties on length scales from about 1 μm up to several millimeters, the films are expected to be poly-crystalline due to the nature of the growth process. A detailed investigation of nanoscale inhomogeneities, including grain size distributions, grain orientations, grain boundaries as well as possible amorphous regions, may provide further insights and a further understanding of the growth process and potential optimization strategies for tunable optoelectronic properties.

Conclusion

In conclusion, we have demonstrated an approach to synthesize MoS_2 thin layers by sulfurization of thermally evaporated MoO_{3-x} precursor layers. Raman and PL spectroscopy confirmed the formation of MoS_2 monolayers above a temperature of 700 °C on Si substrates with native oxide and on 100 nm

SiO_2/Si substrates. We have further investigated possible variations in the process sequence and their influence on the possible reaction pathways for MoS_2 film formation. Our study reveals that, in addition to the process temperature, the delay time for the H_2S injection is a crucial kinetic parameter, which determines the extent of evaporation of the MoO_{3-x} precursor. This ultimately governs the reaction path (solid or vapor phase reaction) and thickness of the resulting MoS_2 layers. The as-grown monolayer samples which were processed in the temperature range of 950–1000 °C exhibit a PL yield on the same quantitative level as exfoliated monolayer flakes.

Conflicts of interest

There are no conflicts to declare.

Acknowledgements

References

1 K. F. Mak, C. Lee, J. Hone, J. Shan and T. F. Heinz, *Phys. Rev. Lett.*, 2010, **105**, 136805.

2 B. Radisavljevic, A. Radenovic, J. Brivio, V. Giacometti and A. Kis, *Nat. Nanotechnol.*, 2011, **6**, 147–150.

3 A. Ayari, E. Cobas, O. Ogundadegbe and M. S. Fuhrer, *J. Appl. Phys.*, 2007, **101**, 014507.

4 J. Zhao, W. Chen, J. Meng, H. Yu, M. Liao, J. Zhu, R. Yang, D. Shi and G. Zhang, *Adv. Electron. Mater.*, 2016, **2**, 1500379.

5 M. Choi, Y. J. Park, B. K. Sharma, S.-R. Bae, S. Y. Kim and J.-H. Ahn, *Sci. Adv.*, 2018, **4**, eaas8721.

6 J. Jeon, S. K. Jang, S. M. Jeon, G. Yoo, Y. H. Jang, J.-H. Park and S. Lee, *Nanoscale*, 2015, **7**, 1688–1695.

7 J. Mann, D. Sun, Q. Ma, J. R. Chen, E. Preciado, T. Ohta, B. Diaconescu, K. Yamaguchi, T. Tran, M. Wurch, K. Magnone, T. F. Heinz, G. L. Kellogg, R. Kawakami and L. Bartels, *Eur. Phys. J. B*, 2013, **86**, 2–5.

8 J. Robertson, X. Liu, C. Yue, M. Escarra and J. Wei, *2D Mater.*, 2017, **4**, 045007.

9 B. Chen, Q. Yu, Q. Yang, P. Bao, W. Zhang, L. Lou, W. Zhu and G. Wang, *RSC Adv.*, 2016, **6**, 50306–50314.

10 Y.-H. Lee, X.-Q. Zhang, W. Zhang, M.-T. Chang, C.-T. Lin, K.-D. Chang, Y.-C. Yu, J. T.-W. Wang, C.-S. Chang, L.-J. Li and T.-W. Lin, *Adv. Mater.*, 2012, **24**, 2320–2325.

11 K. Kang, S. Xie, L. Huang, Y. Han, P. Y. Huang, K. F. Mak, C.-J. Kim, D. Muller and J. Park, *Nature*, 2015, **520**, 656–660.

12 S. Cwik, D. Mitoraj, O. Mendoza Reyes, D. Rogalla, D. Peeters, J. Kim, H. M. Schütz, C. Bock, R. Beranek and A. Devi, *Adv. Mater. Interfaces*, 2018, **5**, 1800140.

13 Y. Kim, J. G. Song, Y. J. Park, G. H. Ryu, S. J. Lee, J. S. Kim, P. J. Jeon, C. W. Lee, W. J. Woo, T. Choi, H. Jung, H. B. R. Lee, J. M. Myoung, S. Im, Z. Lee, J. H. Ahn, J. Park and H. Kim, *Sci. Rep.*, 2016, **6**, 1–8.

14 B. D. Keller, A. Bertuch, J. Provine, G. Sundaram, N. Ferralis and J. C. Grossman, *Chem. Mater.*, 2017, **29**, 2024–2032.

15 D. Dumcenco, D. Ovchinnikov, K. Marinov, P. Lazić, M. Gibertini, N. Marzari, O. L. Sanchez, Y. C. Kung, D. Krasnozhon, M. W. Chen, S. Bertolazzi, P. Gillet, A. Fontcuberta I Morral, A. Radenovic and A. Kis, *ACS Nano*, 2015, **9**, 4611–4620.

16 Y. Kim, H. Bark, G. H. Ryu, Z. Lee and C. Lee, *J. Phys.: Condens. Matter*, 2016, **28**, 184002.

17 H. Liu, K. K. Ansah Antwi, J. Ying, S. Chua and D. Chi, *Nanotechnology*, 2014, **25**, 405702.

18 Y.-C. Lin, W. Zhang, J.-K. Huang, K.-K. Liu, Y.-H. Lee, C.-T. Liang, C.-W. Chu and L.-J. Li, *Nanoscale*, 2012, **4**, 6637.

19 A. Castellanos-Gomez, M. Buscema, R. Molenaar, V. Singh, L. Janssen, H. S. J. Van Der Zant and G. A. Steele, *2D Mater.*, 2014, **1**, 011002.

20 Y. Yu, C. Li, Y. Liu, L. Su, Y. Zhang and L. Cao, *Sci. Rep.*, 2013, **3**, 1866.

21 H. Li, Q. Zhang, C. C. R. Yap, B. K. Tay, T. H. T. Edwin, A. Olivier and D. Baillargeat, *Adv. Funct. Mater.*, 2012, **22**, 1385–1390.

22 Y.-T. Ho, C.-H. Ma, T.-T. Luong, L.-L. Wei, T.-C. Yen, W.-T. Hsu, W.-H. Chang, Y.-C. Chu, Y.-Y. Tu, K. P. Pande and E. Y. Chang, *Phys. Status Solidi RRL*, 2015, **9**, 187–191.

23 L. Liang and V. Meunier, *Nanoscale*, 2014, **6**, 5394–5401.

24 Y. Kim, H. Bark, G. H. Ryu, Z. Lee and C. Lee, *J. Phys.: Condens. Matter*, 2016, **28**, 184002.

25 C. Lee, H. Yan, L. Brus, T. Heinz, J. Hone and S. Ryu, *ACS Nano*, 2010, **4**, 2695–2700.

26 A. M. Van Der Zande, P. Y. Huang, D. A. Chenet, T. C. Berkelbach, Y. You, G. H. Lee, T. F. Heinz, D. R. Reichman, D. A. Muller and J. C. Hone, *Nat. Mater.*, 2013, **12**, 554–561.

27 H.-Y. Liu, U. K. Das and R. W. Birkmire, *Langmuir*, 2017, **33**, 14580–14585.

28 M. Bosi, *RSC Adv.*, 2015, **5**, 75500–75518.

29 A. Özden, F. Ay, C. Sevik and N. K. Perkgöz, *Jpn. J. Appl. Phys.*, 2017, **56**, 06GG05.

30 K. F. Mak, K. He, C. Lee, G. H. Lee, J. Hone, T. F. Heinz and J. Shan, *Nat. Mater.*, 2013, **12**, 207–211.

31 Y. Lin, X. Ling, L. Yu, S. Huang, A. L. Hsu, Y. H. Lee, J. Kong, M. S. Dresselhaus and T. Palacios, *Nano Lett.*, 2014, **14**, 5569–5576.

32 Y. Xie, Z. Wang, Y. Zhan, P. Zhang, R. Wu, T. Jiang, S. Wu, H. Wang, Y. Zhao, T. Nan and X. Ma, *Nanotechnology*, 2017, **28**, 084001.

33 F. Fabbri, E. Rotunno, E. Cinquanta, D. Campi, E. Bonnini, D. Kaplan, L. Lazzarini, M. Bernasconi, C. Ferrari, M. Longo, G. Nicotra, A. Molle, V. Swaminathan and G. Salviati, *Nat. Commun.*, 2016, **7**, 13044.

34 M. K. L. Man, S. Deckoff-Jones, A. Winchester, G. Shi, G. Gupta, A. D. Mohite, S. Kar, E. Kioupakis, S. Talapatra and K. M. Dani, *Sci. Rep.*, 2016, **6**, 20890.

35 Q. Ji, Y. Zhang, Y. Zhang and Z. Liu, *Chem. Soc. Rev.*, 2015, **44**, 2587–2602.

36 V. E. Kaloidas and N. G. Papayannakos, *Int. J. Hydrogen Energy*, 1987, **12**, 403–409.

37 A. N. Startsev, O. V. Kruglyakova, Y. A. Chesalov, S. P. Ruzankin, E. A. Kravtsov, T. V. Larina and E. A. Paukshtis, *Top. Catal.*, 2013, **56**, 969–980.

38 Y. Y. Wen, X. B. Zeng, X. X. Chen, W. Z. Wang, J. Ding and S. E. Xu, in *2nd Annual International Conference on Advanced Material Engineering (AME 2016)*, 2016, pp. 1034–1039.

39 Y. Feldman, E. Wasserman, D. J. Srolovitz and R. Tenne, *Science*, 1995, **267**, 222–225.

40 M. M. Benameur, B. Radisavljevic, J. S. Héron, S. Sahoo, H. Berger and A. Kis, *Nanotechnology*, 2011, **22**, 125706.

41 T. Weber, J. C. Muijsers, J. H. M. C. van Wolput, C. P. J. Verhagen and J. W. Niemantsverdriet, *J. Phys. Chem.*, 1996, **100**, 14144–14150.